Inorg. Chem. **2004**, *43*, 473–481

Coordination Frameworks Containing the Pyrimidin-4-olate Ligand. Synthesis, Thermal, Magnetic, and *ab Initio* XRPD Structural Characterization of Nickel and Zinc Derivatives

Elisa Barea,[†] Jorge A. R. Navarro,*[,†] Juan M. Salas,*[,†] Norberto Masciocchi,*[,‡] Simona Galli,[‡] and Angelo Sironi[§,||]

Departamento de Química Inorgánica, Universidad de Granada, Av. Fuentenueva S/N, E-18071 Granada, Spain, Dipartimento di Scienze Chimiche, Fisiche e Matematiche, Università degli Studi dell'Insubria, via Valleggio 11, I-22100 Como, Italy, Dipartimento di Chimica Strutturale e Stereochimica Inorganica, Università degli Studi di Milano, via Venezian 21, I-20133 Milano, Italy, and Istituto di Scienze e Tecnologie Molecolari del CNR e Istituto Nazionale di Fisica della Materia, via Golgi 19, I-20133 Milano, Italy

Received September 29, 2003

Extended coordination frameworks containing the pyrimidin-4-olate ligand (4-pymo) and Zn(II) and Ni(II) metal ions have been obtained by solid state reactions and have been fully characterized by spectroscopic, thermal, and magnetic measurements and by *ab initio* XRPD. The reaction of ZnO and 4-Hpymo at 140 °C gives a solid microcrystalline phase, $Zn(4\text{-pymo})_2$ (**1**). Its 3D framework contains Zn(II) centers linked by 4-pymo ligands acting in two different coordination modes, namely, the *N*,*N*′- and the *N*,*O*-*exo*-bidentate ones, which result in a pseudotetrahedral ZnN_3O chromophore. Thermal treatment of the "molecular" $Ni(4\text{-pymo})_2(H_2O)_4$ complex (**2**) above 140 °C gives an anhydrous amorphous material analyzing as $Ni(4\text{-pymo})_2$ (**3a**). Further heating of this material above 388 °C results in the formation of the microcrystalline layered $Ni(4\text{-pymo})_2$ species (**3b**), in which Ni(II) centers are bridged by *N*,*O*-*exo*-bidentate 4-pymo ligands (assisted by longer Ni···N contacts). The thermal dependence of the magnetic susceptibility has been studied for the paramagnetic species **2** and **3a**. **2** shows a weak antiferromagnetic interaction [$J = -0.313(5)$ cm^{-1}] transmitted through the multiple H-bonding interactions between the exocyclic pyrimidine and water oxygen atoms coordinated to the metal centers. **3a** behaves as a 2D Heisenberg antiferromagnet with $J = -4.11(3)$ cm^{-1}.

Introduction

The synthesis of solid materials frequently requires high temperature and/or high pressure solid state reactions. This strategy may involve either a single precursor, implying transformation of one phase to another, or reaction of two or more components to give a single product. Although very common in the field of solids of high technological interest, *e.g.* superconductors, semiconductors, and magnetic materials,[1] this synthetic methodology is rarely applied in the preparation of extended coordination compounds.[2,3] A typical consequence of solid state reactions is that microcrystalline powders (not single crystals!) are obtained. Therefore, most researchers employ either crystallization from solution[4] or hydrothermal methods[5] in order to obtain single crystals suitable for conventional structural analysis. However, when

* Authors to whom correspondence should be addressed. E-mail: jarn@ugr.es (J.A.R.N.).
[†] Universidad de Granada.
[‡] Università degli Studi dell'Insubria.
[§] Università degli Studi di Milano.
[||] Istituto di Scienze e Tecnologie Molecolari del CNR e Istituto Nazionale di Fisica della Materia.

(1) Elliot, S. *The Physics and Chemistry of Solids;* John Wiley & Sons: Chichester, 2000.
(2) (a) Masciocchi, N.; Galli, S.; Sironi, A.; Barea, E.; Navarro, J. A. R.; Salas, J. M.; Tabares, L. C. *Chem. Mater.* **2003**, *15*, 2153. (b) Masciocchi, N.; Ardizzoia, G. A.; LaMonica, G.; Maspero, A.; Sironi, A. *Eur. J. Inorg. Chem.* **2000**, 2507. (c) Tabares, L. C.; Navarro, J. A. R.; Salas, J. M. *J. Am. Chem. Soc.* **2001**, *123*, 383.
(3) (a) Kitaura, R.; Seki, K.; Akiyama, G.; Kitagawa, S. *Angew. Chem., Int. Ed.* **2003**, *42*, 428. (b) Kitaura, R.; Fujimoto, K.; Noro, S.-I.; Kondo, M.; Kitagawa, S. *Angew. Chem., Int. Ed.* **2002**, *41*, 133. (c) Virada, K.; Fujita, M. *Angew. Chem., Int. Ed.* **2002**, *41*, 3392. (d) Virada, K.; Hongo, Y.; Fujita, M. *Angew. Chem., Int. Ed.* **2002**, *41*, 3395. (e) Soldatov, D. V.; Ripmeester, J. A.; Shergina, S. I.; Sokolov, I. E.; Zanina, A. S.; Gromilov, S. A.; Dyadin, Y. A. *J. Am. Chem. Soc.* **1999**, *121*, 4179. (f) Bourne, S. A.; Kilkenny, M.; Nassimbeni, L. R. *J. Chem. Soc., Dalton Trans.* **2001**, 1176.

10.1021/ic0351287 CCC: $27.50
Published on Web 12/23/2003

Chart 1

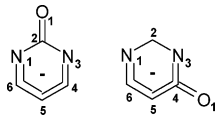

single crystals lack, microcrystalline powders can be conveniently characterized using *ab initio* X-ray powder diffraction (XRPD) which, in the recent past, has been shown to afford limited, but otherwise inaccessible, structural information.[6]

We are currently interested in the coordination chemistry of 2-hydroxypyrimidine (2-Hpymo) and 4-hydroxypyrimidine (4-Hpymo), see Chart 1, which are ideally suited for the construction of extended coordination frameworks with rich structural,[7] thermal,[8] magnetic,[2a] and sorptive[2c,9] properties. In the present contribution, we describe Ni, 2D-, and Zn, 3D-polymers, based on the versatile 4-pymo ligand, and show the suitability of XRPD for their structural characterization.

Experimental Section

General Methods. 4-Hydroxypyrimidine (4-Hpymo, from Aldrich Chemical Co.) and the other chemical reagents and solvents were acquired from available commercial sources and used as received. IR absorption bands were measured by a Midac FT-IR on KBr pellets. Electronic spectra of solid samples were carried out on a Varian Cary UV−vis−NIR spectrophotometer, and thermogravimetric and differential scanning calorimetric analyses were performed, under dinitrogen, on Shimadzu-TGA-50H/DSC equipment, at heating rates of 10 °C min^{-1} and 5 °C min^{-1}, respectively (Scientific Instrumentation Center of the University of Granada). Magnetic susceptibility measurements were performed on polycrystalline samples with a Quantum Design MPMS-2SQUID magnetometer (Complutense University) operating in the temperature range 2−300 K and at a magnetic field strength of 10 kG.

Preparation of Zn(4-pymo)$_2$, 1. ZnO (1.5 mmol) and an excess of 4-Hpymo (6 mmol) were ground in an agate mortar and heated at 140 °C for 2 h under N_2 atmosphere. To eliminate the unreacted 4-Hpymo, the crude product was suspended in acetone (40 mL) and stirred at room temperature for 2 h. The resulting cream-white microcrystalline material was washed with acetone and dried in air. Yield: 95%. Anal. Calcd for $C_8H_6N_4O_2Zn\cdot(ZnO)_{1/5}$: C, 35.35; H, 2.22; N, 20.61. Found: C, 35.1; H, 2.3; N, 20.4. IR (selected bands in cm^{-1}): 1655 vs, 1607 vs, 1541 s, 1498 m, 1479 s, 1424 s, 1377 m, 1352 m, 1160 m, 1055 m, 889 m, 844 s. UV−vis (nm): 220 vs, 260 vs.

Preparation of Ni(4-pymo)$_2$(H$_2$O)$_4$, 2. An aqueous solution (40 mL) containing 4-Hpymo (4 mmol) and NaOH (4 mmol) was added dropwise into an aqueous solution of $Ni(AcO)_2\cdot 6H_2O$ (2 mmol). The resulting suspension was stirred at room temperature for 2 h affording a pale blue-green microcrystalline material, which was washed with ethanol and diethyl ether and dried in air. Yield: 90%. Anal. Calcd for $C_8H_{14}N_4O_6Ni$: C, 29.94; H, 4.40; N, 17.46. Found: C, 29.8; H, 4.6; N, 17.4. IR (selected bands in cm^{-1}): 1607 vs, 1520 s, 1477 s, 1418 vs, 1329 s, 1022 s, 837 br, s. UV−vis (nm): 228 vs, 268 vs, 388 m, 640 m, 1050 br, m.

Preparation of Ni(4-pymo)$_2$, 3a (Amorphous Phase) and 3b (Crystalline Phase). 200 mg of **2** was heated at 140 °C for 2 h, affording a green amorphous phase of Ni(4-pymo)$_2$ formula (**3a**). Anal. Calcd for $C_8H_6N_4O_2Ni$: C, 38.61; H, 2.43; N, 22.51. Found: C, 38.1; H, 2.5; N, 22.2. IR (selected bands in cm^{-1}): 1611 vs, 1541 s, 1483 s, 1425 s, 1366 m, 1331 m, 1020 m, 839 m. UV−vis (nm): 220 vs, 268 vs, 395 s, 652 s, 1140 s, br. Further heating of 30 mg of **3a** under dinitrogen at a heating rate of 10 °C min^{-1} up to 385 °C and then keeping it at this temperature during 5 min afforded a green microcrystalline material (**3b**). Anal. Calcd for $C_8H_6N_4O_2Ni\cdot(NiO)_{1/5}$: C, 36.43; H, 2.29; N, 21.24. Found: C, 36.3; H, 2.4; N, 21.1. IR (selected bands in cm^{-1}): 1609 vs, 1539 s, 1485 s, 1421 s, 1365 m, 1327 m, 1015 m, 841 m. UV−vis (nm): 210 vs, 270 vs, 390 s, sh, 650, 1120 s, br.

X-ray Powder Diffraction Analysis of Zn(4-pymo)$_2$, 1, Ni(4-pymo)$_2$(H$_2$O)$_4$, 2, and Ni(4-pymo)$_2$, 3b. The powders were gently ground in an agate mortar and then cautiously deposited in the hollow of an aluminum holder equipped with a zero background plate (supplied by The Gem Dugout, State College, PA). Diffraction data (Cu Kα, $\lambda = 1.5418$ Å) were collected on a θ:θ Bruker AXS D8 diffractometer equipped with primary and secondary Soller slits (2.3°), divergence, antiscatter, and receiving slits (0.5°, 0.5°, and 0.2 mm, respectively), secondary beam curved graphite monochromator, Na(Tl)I scintillation detector, and pulse height amplifier discrimination. The generator was operated at 40 kV and 40 mA. Nominal resolution for the present setup is 0.07° 2θ (fwhm of the α_1 component) as measured from the Si(111) peak at 28.44° (2θ). Long step-scans with $\Delta 2\theta = 0.02°$ were performed in the ranges $5 < 2\theta < 105°$ with $t = 30$ s.

For **1** and **3b**, indexing was obtained with TREOR90[10] [**1**, monoclinic, $a = 11.43$, $b = 10.52$, $c = 7.17$ Å, $\beta = 122.1°$, $M(18)$[11] $= 29$, $F(18)$[12] $= 52(0.010, 35)$; **3b**, tetragonal, $a = 6.51$, $c = 20.93$ Å, $M(11) = 39$, $F(11) = 29(0.007, 55)$]. The reduced cell of **1** was transformed into the correct trigonal one using the LEPAGE program.[13] Systematic absences prompted for, among others, *R*3*c* and *I*4$_1$/*amd* as suitable space groups for **1** and **3b**, respectively, later confirmed by successful structure solutions and refinements. Noteworthy, the *very slight* splitting of the *tetragonal* [0 2 0] peak into the *orthorhombic* [2 0 0] and [0 2 0] ones, observed in its cobalt analogue,[2a] could not be evidenced in the XRPD trace of **3b**, which was definitely considered tetragonal. As regards **2**, visual inspection of its XRPD trace suggested its strict isomorphous character with the previously reported Co(4-pymo)$_2$(H$_2$O)$_4$,[2a] eventually supported by successful structure refinement. For **1** and **3b**, whole profile

(4) (a) Zawarotko, M. J. *Chem. Commun.* **2001**, 1. (b) Noro, S.-I.; Kitaura, R.; Kondo, M.; Kitagawa, S.; Ishii, T.; Matsuzaka, H.; Yamashita, M. *J. Am. Chem. Soc.* **2002**, *124*, 2568. (c) Beauvais, L. G.; Long, J. R. *J. Am. Chem. Soc.* **2002**, *124*, 12096. (d) Eddaoudi, M.; Kim, J.; Rosi, N.; Vodak, D.; Wachter, J.; O'Keeffe, M.; Yaghi, O. M. *Science* **2002**, *295*, 469. (e) Colacio, E.; Kivekäs, R.; Lloret, F.; Sundberg, M.; Suarez-Varela, J.; Bardají, M.; Laguna, A. *Inorg. Chem.* **2002**, *41*, 5141.

(5) (a) Hagrman, P.; Hagrman, D.; Zubieta, J. *Angew. Chem., Int. Ed.* **1999**, *38*, 2638. (b) Evans, R. V.; Xiong, R.-E.; Wang, Z.; Wong, G. K.; Lin, W. *Angew. Chem., Int. Ed.* **1999**, *38*, 536.

(6) (a) Masciocchi, N.; Sironi, A. *J. Chem. Soc., Dalton Trans.* **1997**, 4643. (b) David, W. I. F.; Shankland, K.; McCusker, L. B.; Baerlocher, Ch. *Structure Determination from Powder Diffraction Data*; Oxford University Press: New York, 2002.

(7) (a) Masciocchi, N.; Ardizzoia, G. A.; LaMonica, G.; Maspero, A.; Sironi, A. *Angew. Chem., Int. Ed.* **1998**, *37*, 3366. (b) Navarro, J. A. R.; Freisinger, E.; Lippert, B. *Inorg. Chem.* **2000**, *39*, 1059. (c) Quirós, M. *Acta Crystallogr.* **1994**, *C50*, 1236.

(8) Masciocchi, N.; Corradi, E.; Moret, M.; Ardizzoia, G. A.; Maspero, A.; LaMonica, G.; Sironi, A. *Inorg. Chem.* **1997**, *36*, 5648.

(9) Barea, E.; Navarro, J. A. R.; Salas, J. M.; Masciocchi, N.; Galli, S.; Sironi, A. *Polyhedron* **2003**, *22*, 3051.

(10) Werner, P. E.; Eriksson, L.; Westdahl, M. *J. Appl. Crystallogr.* **1985**, *18*, 367.

(11) De Wolff, P. M. *J. Appl. Crystallogr.* **1968**, *1*, 108.

(12) Smith, G. S.; Snyder, R. L. *J. Appl. Crystallogr.* **1979**, *12*, 60.

(13) Le Page, Y. *J. Appl. Crystallogr.* **1982**, *15*, 255.

Table 1. Summary of Crystal Data and Data Analysis Parameters for **1**, **2**, and **3b**[a]

compound	**1**	**2**	**3b**
method	XRPD	XRPD	XRPD
formula	$C_8H_6ZnN_4O_2$	$C_8H_{14}NiN_4O_6$	$C_8H_6NiN_4O_2$
fw, g mol^{-1}	255.54	320.91	248.85
system	trigonal	orthorhombic	tetragonal
space group	*R*3*c*	*Pcab*	*I*4$_1$/*amd*
a, Å	21.0415(4)	13.4276(4)	6.5141(7)
b, Å	21.0415(4)	12.9033(5)	6.5141(7)
c, Å	11.4294(2)	6.7550(2)	20.931(3)
Z	18	4	4
V, Å^3	4832.3(2)	1170.4(1)	888.2(2)
ρ_{calc}, g cm^{-3}	1.743	1.776	2.148
F(000)	2304	632	592
μ(Cu Kα), cm^{-1}	34.15	27.34	33.35
diffractometer	Bruker AXS D8	Bruker AXS D8	Bruker AXS D8
T, K	298(2)	298(2)	298(2)
2θ range, deg	5−105	10−105	10−80
N_{data}	5000	4750	3500
N_{obs}	559	668	89
R_p, R_{wp}	0.064, 0.083	0.087, 0.113	0.073, 0.099
R_B	0.025	0.070	0.031
χ^2	2.36	3.21	2.02

[a] $R_p = \sum_i|y_{i,o} - y_{i,c}|/\sum_i|y_{i,o}|$; $R_{wp} = [\sum_i w_i(y_{i,o} - y_{i,c})^2/\sum_i w_i(y_{i,o})^2]^{1/2}$; $R_B = \sum_n||I_{n,o}| - |I_{n,c}||/\sum_i|I_{n,o}|$; $\chi^2 = \sum_i w_i(y_{i,o} - y_{i,c})^2/(N_{obs} - N_{par})$, where $y_{i,o}$ and $y_{i,c}$ are the observed and calculated profile intensities, respectively, while $|F_{n,o}|$ and $|F_{n,c}|$ are the observed and calculated structure factors. The summations run over *i* data points or *n* independent reflections. Statistical weights w_i are normally taken as $1/y_{i,o}$.

structure solutions using simulated annealing[14] were performed with the TOPAS 2.0 suite of programs.[15] 4-pymo ligands were treated as rigid bodies, assigning average literature bond distances and angles (C−C and C−N distances = 1.40 Å; C−O distance = 1.25 Å; C−H distances = 0.95 Å; ring bond angles = 120.0°). The final refinements were performed by the Rietveld method using TOPAS, maintaining the rigid bodies described above. In the hydrated species **2**, even the crystallographically independent Ni(O$_w$)$_2$ moiety (O$_w$ = coordinated water oxygens) was treated as a rigid body (Ni−O$_w$ 2.10 Å, O$_w$−Ni−O$_w$ 90.0°). Peak shapes were described by the fundamental parameters approach.[16] The experimental background was fitted by a polynomial description. Systematic errors were modeled with sample-displacement angular shifts, preferred orientation corrections in the March−Dollase[17] formulation (with [001] and [010] poles in **1** and **2**, respectively), and anisotropic peak shape broadening (**3b**).[16] Metal atoms were given a refinable, isotropic displacement parameter (B_M), while lighter atoms were assigned a common $B = B_M + 2.0$ Å^2 value. Scattering factors, corrected for real and imaginary anomalous dispersion terms, were taken from the internal library of TOPAS. Final R_p, R_{wp}, R_B, and χ^2 agreement factors, together with details on the data collections and analyses for **1**, **2**, and **3b**, can be found in Table 1. Figure 1a−c shows the final Rietveld refinement plots. Relevant structural parameters can be found throughout the text or in the figure captions. Final fractional coordinates are supplied as Supporting Information. Crystallographic data (excluding structure factors) for the three structures reported in this paper have been deposited with the Cambridge Crystallographic Data Centre as supplementary publication numbers CCDC 220369−220371. Copies of the data can be obtained free of charge on application to CCDC, 12 Union Road, Cambridge CB2 1EZ, U.K. [fax, (+44)-1223 336-033; e-mail, deposit@ccdc.cam.ac.uk].

Results

Synthesis and Spectroscopy. Reaction at 140 °C in an open vessel of powdered ZnO and an excess of 4-hydroxypyrimidine (4-Hpymo) gives rise to the formation of a cream-white slurry that, after removal of unreacted 4-Hpymo, yields a cream-white microcrystalline Zn(4-pymo)$_2$ phase (**1**). It should be noted that the reaction conditions are well below the melting point of 4-hydroxypyrimidine (164.5 °C), which makes this process a clear example of a two component solid to solid reaction. The resulting material is, however, only thermally stable up to 285 °C (see Figure 2), which is surprisingly low, especially considering the high thermal stability of the related Zn(2-pymo)$_2$ (T_{dec} = 570 °C).[2b]

Reaction of 4-hydroxypyrimidine and nickel(II) salts in aqueous media gives the pale blue-green and poorly soluble microcrystalline Ni(4-pymo)$_2$(H$_2$O)$_4$ material (**2**). The water content of **2** has been confirmed by thermogravimetric and differential scanning calorimetric analyses (see Figure 2), showing that the four water molecules are lost in a single-step endothermic process at about 150 °C ($\Delta H = -205$ kJ mol^{-1}) giving rise to the anhydrous green amorphous Ni(4-pymo)$_2$ material (**3a**). Further heating of this sample promotes recrystallization (onset at 388 °C, $\Delta H = 9.9$ kJ mol^{-1}) into the microcrystalline Ni(4-pymo)$_2$ phase (**3b**). The latter process overlaps with the onset of a further decomposition event, yielding NiO as the final product, which makes it impossible to obtain **3b** as a 100% pure sample.[18] The presence of the NiO impurity on the crystalline sample is, however, not shown by the XRPD studies, which may be due to the presence of a highly dispersed oxide material. The thermal stability of these systems is significantly lower than that of the previously reported Co(4-pymo)$_2$ (T_{dec} = 470 °C)[2a] and related M(2-pymo)$_2$ complexes, which are stable above 500 °C.[2b]

IR spectra of the samples are indicative of the structural features of these systems (*vide infra*). Thus, the ν(CO) vibration modes of **1** agree with the simultaneous occurrence of two types of coordination for the 4-pymo ligand, manifested by the strong 1655 and 1607 cm^{-1} absorption bands. The former absorption can be attributed to the uncoordinated nature of the exocyclic oxygen atom of one of the 4-pymo ligands (showing *N*,*N*′-coordination), while the lower frequency peak clearly implies O$_1$ coordination, with the simultaneous weakening of the pertinent C=O$_1$ bond. IR spectra also substantiate the changes taking place on passing from **2** to **3a**. The relative small shift of the ν(CO) vibration mode, from 1607 to 1611 cm^{-1} after O$_1$ involvement in metal coordination, can be attributed to the presence of strong H-bonding interactions in **2** (see below). The **3a** to **3b** transformation is not accompanied by any shift of the IR absorption bands; indeed, only their sharpening is observed. This fact prompts for their closely related nature.

(14) Coelho, A. A. *J. Appl. Crystallogr.* **2000**, *33*, 899.
(15) Bruker AXS 2000: Topas V2.0: General profile and structure analysis software for powder diffraction data.
(16) Cheary, R. W.; Coelho, A. A. *J. Appl. Crystallogr.* **1992**, *25*, 109.
(17) March, A. *Z. Kristallogr.* **1932**, *81*, 285. Dollase, W. A. *J. Appl. Crystallogr.* **1987**, *19*, 267.
(18) Thermal and elemental analyses suggest the presence of *ca*. 6% NiO on the sample.

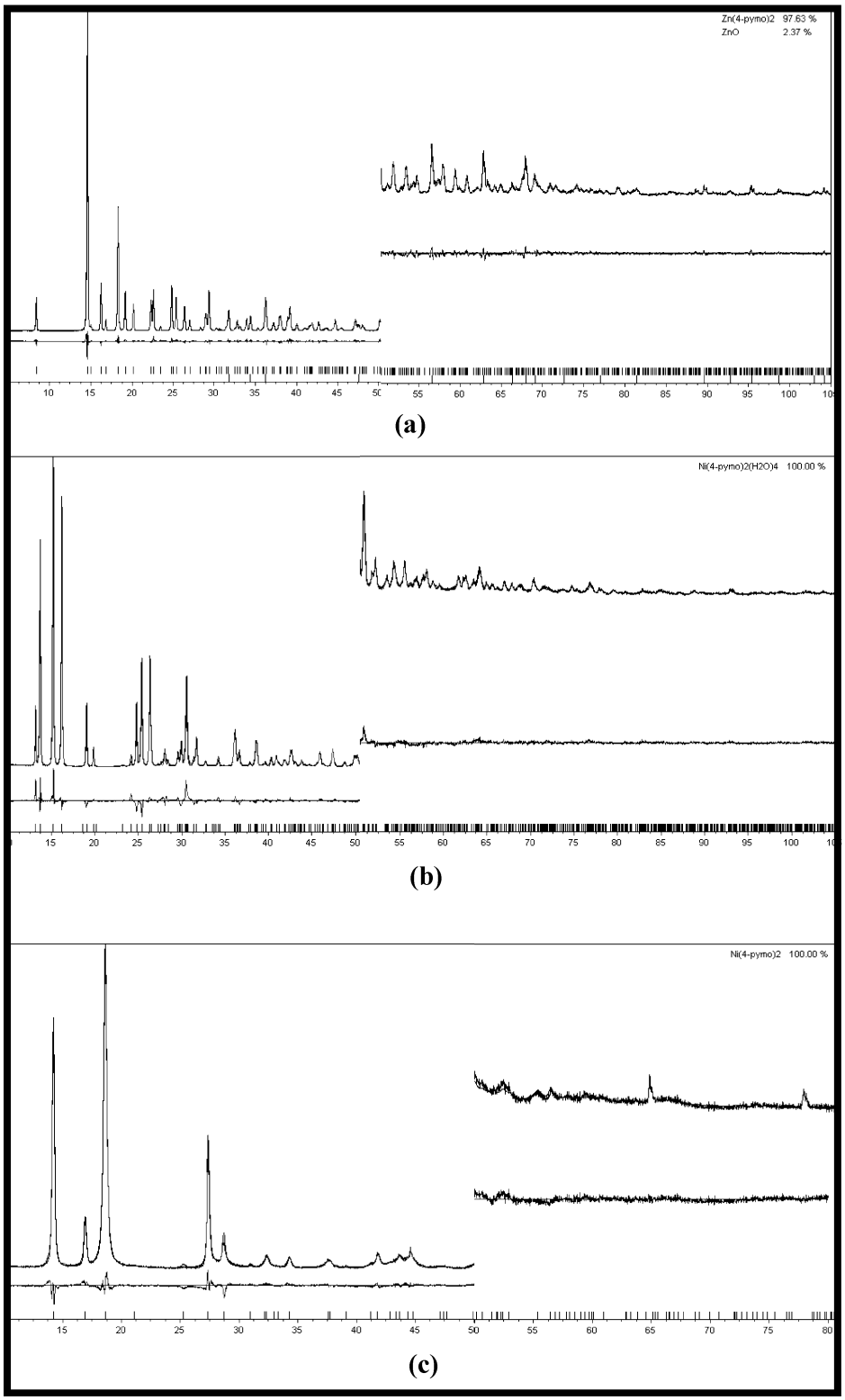

Figure 1. Rietveld refinement plots for **1** (a), **2** (b), and **3b** (c) with difference plots and peak markers at the bottom. Vertical axis, counts (arbitrary units). The section above 50° 2θ has been magnified (10×).

The electronic spectra of **2**, **3a** and **3b** systems are typical of Ni(II) species in similar octahedral environments.[19] Significant differences are, however, present between the spectra of **2** and **3a**. A shift of the d−d absorption bands (reflected by an appreciable color change from pale blue to green) is observed along with a concomitant rise in their intensity. These changes are reflected in the Δ_o values calculated using the Dou method,[20] which gives values of 9525 and 8930 cm^{-1} for **2** and **3a**, respectively. The

(19) Orihuela, S.; Sánchez, M. P.; Quiros, M.; Martín, D.; Faure, R. *Polyhedron* **1998**, *17*, 2477.

(20) Dou, Y. *J. Chem. Educ.* **1990**, *67*, 134.

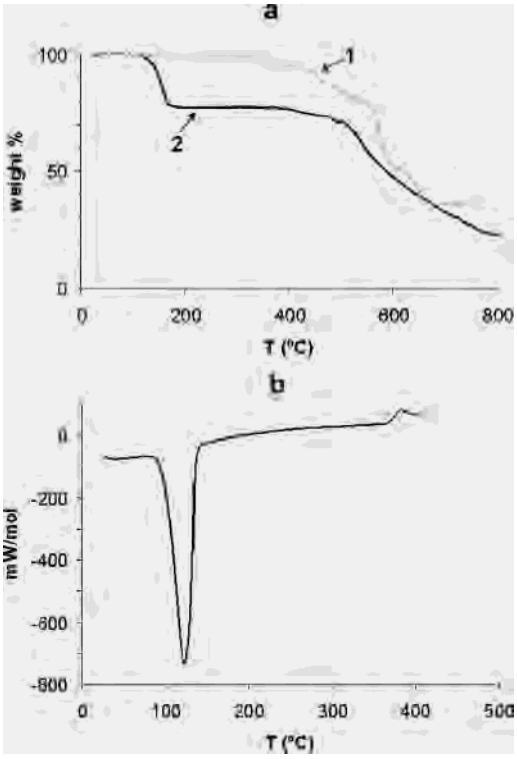

Figure 2. TGA traces for compounds **1** and **2** (a) and DSC trace for compound **2** (b) under N_2 atmosphere.

differences in both the Δ_o values and the intensity of the electronic spectra bands can be attributed to a change of the coordination environment from a *trans*-D_{4h} (forbidden transitions) to a *cis*-C_{2v} (allowed transitions) pseudooctahedral geometry. Additionally, the electronic spectra of **3b** show a broadening of the charge transfer bands (with respect to **3a),** which may be attributed to the presence of impurities (see above).

Crystal Chemistry. Structure of Zn(4-pymo)$_2$, 1. Among the structures here reported, **1** is the most surprising one. Indeed, it was found to contain, in the highly symmetric *R*3*c* space group, one zinc(II) ion (in a general position), surrounded by two crystallographically independent 4-pymo ligands: one bridges metal ions (about 5.72 Å apart) in the common *N*,*N*′-*exo*-bidentate mode, as found, for example, in Zn(2-pymo)$_2$,[2b] while the other shows *N*,*O*-*exo*-bidentate coordination (Zn···Zn ca. 7.05 Å). Thus, each zinc ion lies in a nearly tetrahedral N_3O environment [Zn−N = 1.958(7), 2.036 (8), and 2.046(7) Å; Zn−O = 2.023(13) Å; N−Zn−N = 106.0(4), 110.2(4), and 121.0(2)°; N−Zn−O = 94.5(4), 107.5(6), and 114.3(5)°] of four different ligands (see Figure 3e).

Interestingly, the *N*,*N*′-bound 4-pymo ligands generate, with the zinc ions, parallel rods of $[Zn_n(4\text{-pymo})_n]^{n+}$ formulation, elongated along *c*, which are interconnected in a 3D network by *N*,*O*-bridges nearly in plane with *ab*. At a supramolecular level, the complex structure of **1** can be idealized, neglecting the nature and the orientation of the 4-pymo ligands, as an *unprecedented* $6_26_26_28_26_36_3$ network (C_{10} = 426),[21] built upon polyconnected tetrahedral nodes. Figure 4a shows a portion of the crystal structure, while Figure 4b contains a sketch of the network. Thus, the isomeric forms of Zn(*X*-pymo)$_2$ (*X* = 2 or 4) show rather distinct framework geometries, single diamondoid for *X* = 2,[2b] and an unprecedented uninodal network for *X* = 4. At variance, the highly porous Cu(*X*-pymo)$_2$ species (*X* = 2, 4), capable of reversible sorption of a number of gases or ions (without changing their framework structure), crystallize, in the cubic $Pn\bar{3}m$ space group, as strictly isomorphous materials.[2c,9]

Structure of Ni(4-pymo)$_2$(H$_2$O)$_2$, 2. This species is strictly isomorphous with the cobalt analogue and, as already discussed in ref 2a for the latter, contains mononuclear ions of pseudooctahedral geometry, bearing four water molecules and two, mutually *trans*, 4-pymo ligands bound through their N_1 atoms. The swinging ends of the organic ligands are involved in an extended network of hydrogen bonds (through the N_3 and exocyclic oxygen atoms); accordingly, these "three-dimensional H-bonded polymers" are rather insoluble species. A sketch of the monomer in **2** is shown in Figure 5, together with some pertinent geometrical parameters.

Structure of Crystalline Ni(4-pymo)$_2$, 3b. This species contains two-dimensional infinite layers of square meshes, where the nickel(II) ions (separated by 6.51 Å, *i.e.* **a** or **b**) are the nodes and the 4-pymo ligands, bridging in the *N*,*O*-*exo*-bidentate mode, the rungs. Refined Ni−N_1 and Ni−O_1 bond distances have values of 1.97(1) and 2.08(2) Å, respectively. The (*N*,*O*-bridged) M···M distance in **3b**, significantly shorter than in **1**, can be explained by the presence of an ancillary Ni···N_3 contact [2.29(1) Å], making each Ni(II) ion *hexa*-, not just *tetra*-coordinated. Crystal packing of **3b** is shown in Figure 6, where the long Ni···N_3 are dashed.

As already discussed for the related Co(4-pymo)$_2$,[2a] **3b** shows an extended disorder in the orientation of the 4-pymo ligands; namely: (i) within each layer, all (4-pymo) ligands are rigorously ordered, with a *polar* head-to-tail sequence of the *N*,*O*-bridges, within each rung (running along *a* or *b*), for obvious stereochemical reasons; (ii) each rung is, however, independent and may, or may not, adopt the same polarity of the adjacent ones; in addition, (iii) loss of coherence in the 4-pymo orientation is also caused by the disordered stacking of the layers along *c*. Thus, the highly symmetric $I4_1/amd$ space group results from this multiple disordering effect; for the reader, an ordered structure is drawn by dramatically lowering the crystal symmetry, for example down to $I\bar{1}$ (with the aid of a second, crystallographically independent 4-pymo ligand obtained by the 0.25 − *y*, 0.25 + *x*, 1.75 − *z* transformation, Figure 6). Note that this choice, which clearly implies a *periodic*, but *arbitrary*, sequence of layers along *c*, is by no means unique.

Moreover, it is worthy of note that the still uninterpreted *orthorhombic*, *nearly tetragonal*, lattice observed in Co(4-

(21) (a) Wells, A. F. *Three-dimensional Nets and Polyhedra*; Wiley: New York, 1977. (b) Wells, A. F. *Further Studies of Three-dimensional Nets*; ACA monograph, 8, 1979. (c) O'Keeffe, M.; Hyde, B. G. *Crystal Structures I: Patterns and Symmetry*; Mineral. Soc. Am.: Washington, 1996.

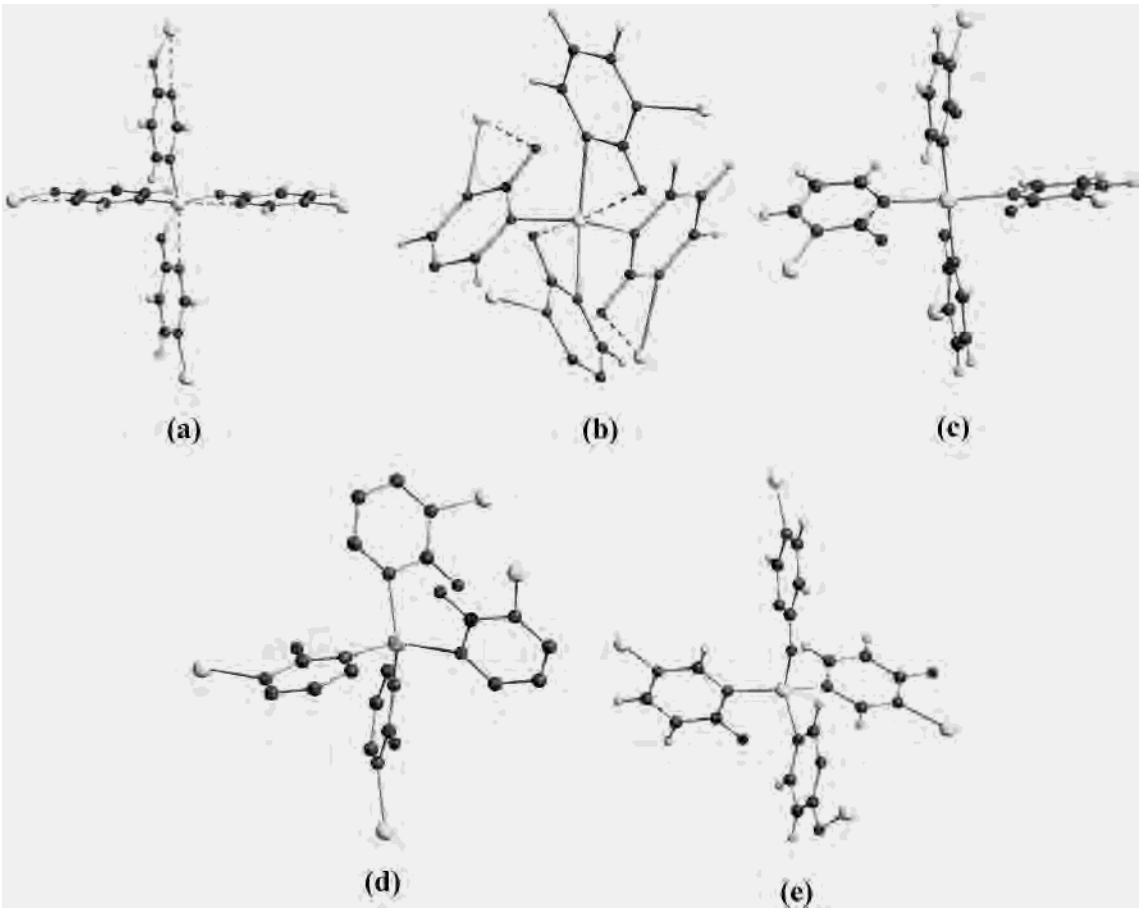

Figure 3. Schematic drawing of $M_5(X\text{-pymo})_4$ fragments in known $M(X\text{-pymo})_2$ compounds ($X = 2$ or 4): (a) $Co(4\text{-pymo})_2$ [$Ni(4\text{-pymo})_2$ is, at the drawing level, identical]; (b) $Ni(2\text{-pymo})_2$; (c) $Cu(4\text{-pymo})_2$ [$Cu(2\text{-pymo})_2$ is, apart from the location of the O_1 atom, practically identical]; (d) $Zn(2\text{-pymo})_2$ [$Co(2\text{-pymo})_2$ is, at the drawing level, identical]; (e) $Zn(4\text{-pymo})_2$. Metal atoms, large spheres in light gray. Carbon, nitrogen, and oxygen atoms, medium spheres in gray. Hydrogen atoms, small spheres in light gray.

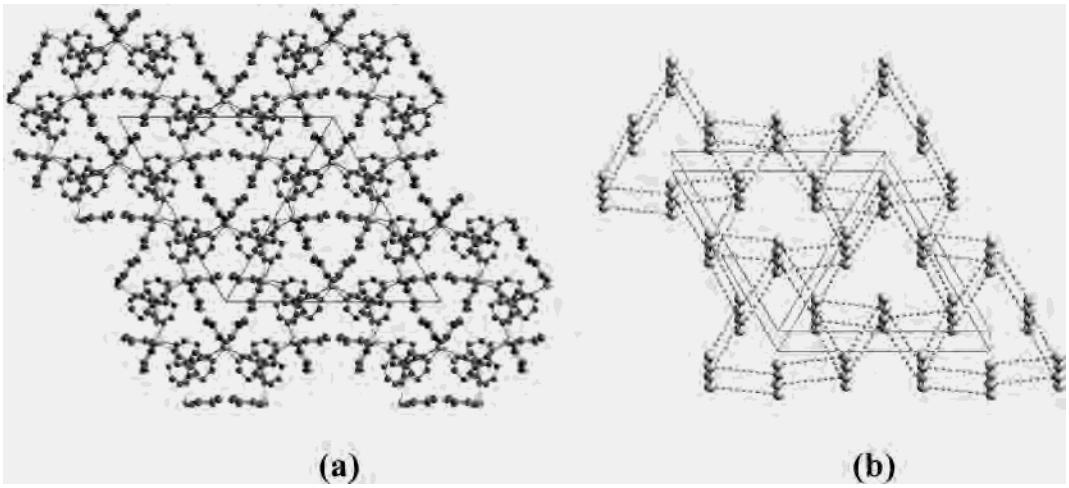

Figure 4. Drawing of (a) crystal packing of $Zn(4\text{-pymo})_2$ in the *R*3*c* space group viewed down [001]; hydrogen atoms omitted for clarity; (b) the supramolecular network of metal ions and their *N*,*N*′- and *N*,*O*-4-pymo bridges, viewed *approximately* down [001]. As idealized in panel b, columns of Zn atoms, running along *c*, are bridged by "conventional" *N*,*N*′-4-pymo ligands, while *N*,*O*-4-pymo fragments lie approximately in planes parallel to *ab* [see panel a]. Zinc atoms, large spheres in light gray. Carbon, nitrogen, and oxygen atoms, medium spheres in gray. Hydrogen atoms omitted for clarity.

$pymo)_2$[2a] is not observed for **3b**, which, thus, behaves regularly, with *a* and *b* rungs of equal periodicity.

Magnetic Characterization. The thermal behavior of χ_M (molar susceptibility per nickel atom) and μ_{eff} (effective moment per nickel atom) for compounds **2** and **3a** is shown in Figure 7. The χ_M values steadily increase upon cooling; however, in the case of compound **2**, they are much higher than in **3a**. The different behavior can be more clearly appreciated from the μ_{eff} values, which are almost constant for **2** above 60 K. At this temperature, μ_{eff} starts to decrease, which is indicative of an antiferromagnetic intermolecular interaction taking place between the $Ni(4\text{-pymo})_2(H_2O)_4$

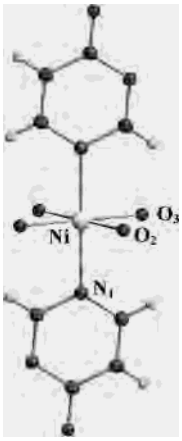

Figure 5. Schematic drawing of the $Ni(4\text{-pymo})_2(H_2O)_4$ molecule, lying on an inversion center. Nickel atoms, large spheres in light gray. Carbon, nitrogen, and oxygen atoms, medium spheres in gray. Hydrogen atoms, small spheres in light gray. Chemically relevant bond distances (Å) and angles (deg): $Ni-N_1$ 2.084(3); N_1-Ni-O_2 90.0(3), N_1-Ni-O_3 88.5(4).

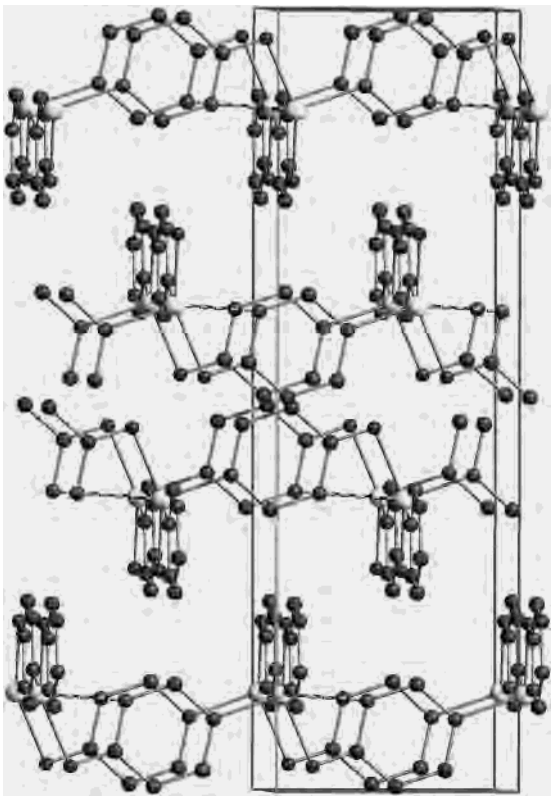

Figure 6. Crystal packing of $Ni(4\text{-pymo})_2$, **3b**, in the idealized $I\bar{1}$ space group (see text). Nickel atoms, large spheres in light gray. Carbon, nitrogen, and oxygen atoms, medium spheres in gray. Hydrogen atoms omitted for clarity. For a detailed view of a single layer, see Figure 3 in ref 2a.

monomers. In the case of **3a**, μ_{eff} steadily decreases upon cooling, which can be related to its polymeric nature, implying a stronger antiferromagnetic exchange taking place between the heavily distorted *pseudo*octahedral metal centers.

The magnetic behavior of **2** has been fitted to the Curie–Weiss law,[22] giving a Weiss temperature value of −2.15 K. This can be related to weak intermolecular antiferromagnetic interactions transmitted through the strong H-bonding interactions established between coordinated water molecules and N_3 and O_1 atoms of pyrimidine moieties.

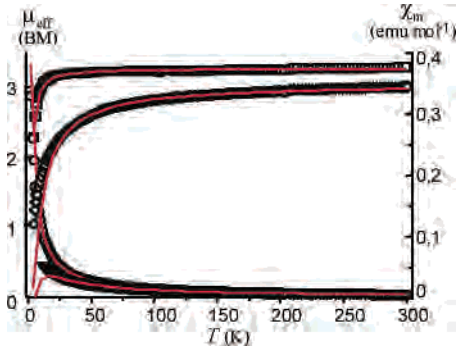

Figure 7. Field cooled χ_m values for **2** (○) and **3a** (▽); μ_{eff} values for **2** (□) and **3a** (◇) in the 2−300 K temperature range and a field strength of 10 kG. Solid lines are the best fit of experimental values to eq 1.

In the case of **3a** and presuming its closely related nature to the **3b** phase,[23] its magnetic behavior can be conveniently described by eq 1, which is adequate for the description of

$$\chi = \frac{Ng^2\mu_B{}^2}{J\left(3\theta + \sum_{n=1}^{\infty}\frac{C_n}{\theta^{n-1}}\right)} \qquad (1)$$

the high temperature dependence of the magnetic susceptibility on a 2D Heisenberg quadratic-layer antiferromagnet,[24] where the spin Hamiltonian is defined as $H = \sum JS_i \cdot S_j$, $\theta = kT/JS(S+1)$, g is the Landé g factor, μ_B is the Bohr magneton, and N is the number of spins in the lattice. The C_n coefficients have been taken from ref 24. Fitting the data to eq 1 gives a value of $g = 2.143(1)$ and an exchange value $J = -4.11(3)$ cm^{-1}, which agrees with a significant antiferromagnetic interaction being transmitted through the pyrimidin-4-olate bridges between adjacent nickel(II) centers. For comparative reasons and taking into account that even **2**, by means of the hydrogen bond network, can be considered an extended material, we have also fitted its magnetic data to eq 1. The results show a reasonable good fitting with $g = 2.304(1)$ and $J = -0.313(5)$ cm^{-1}, which agrees with a small antiferromagnetic interaction being transmitted through the H-bonding interactions between adjacent nickel(II) centers.

Discussion

Table 2 synoptically collects the main features of the recently characterized $M(X\text{-pymo})_2$ species ($X = 2$ or 4), which are discussed hereafter.

Comparative Analysis of the Thermal and Magnetic Properties. The thermal behavior of **2** is closely similar to that of the isomorphous $[Co(4\text{-pymo})_2(H_2O)_4]$[2a] material. Indeed, the dehydration process that leads to the formation of an amorphous phase of type $M(4\text{-pymo})_2$ and the posterior recrystallization to crystalline $M(4\text{-pymo})_2$ materials are very

(22) Mabbs, F. E.; Machin, D. J. *Magnetism and Transition Metal Complexes*; Chapman and Hall: London, 1973.

(23) We avoid including the magnetic behavior of **3b** due to the impossibility of obtaining it as a pure material.

(24) (a) Lines, M. E. *J. Phys. Chem. Solids* **1970**, *31*, 101. (b) Rushbrooke, G. S.; Wood, P. J. *Mol. Phys.* **1958**, *1*, 257.

Table 2. Collection of Structural Parameters for the Known M(X-pymo)$_2$ Species (X = 2 or 4)

	Co(2-pymo)$_2$	Co(4-pymo)$_2$	Ni(2-pymo)$_2$	Ni(4-pymo)$_2$ **3b**	Cu(2-pymo)$_2$[d]	Cu(4-pymo)$_2$[e]	Zn(2-pymo)$_2$	Zn(4-pymo)$_2$ **1**
ref	2b	2a	2b	this work	2c	9	2b	this work
topology	3D diamondoid	2D square meshes	3D diamondoid	2D square meshes	3D sodalite	3D sodalite	3D diamondoid	3D new
space group	$I\bar{4}2d$	*Imma*	*Fdd*2	$I4_1/amd$	$Pn\bar{3}m$	$Pn\bar{3}m$	$I\bar{4}2d$	*R*3*c*
V/Z, Å^3	235	225	217	222	326	326	237	268
metal geometry	MN_4 tetrahedral	MN_4O_2 pseudo-octahedral	MN_4O_2 pseudo-octahedral	MN_4O_2 pseudo-octahedral	MN_4 square planar	MN_4 square planar	MN_4 tetrahedral	MN_3O tetrahedral
M···M, Å	5.65	6.52−6.57	5.46	6.51	5.57	5.57	5.70	5.72, 7.05
pymo bridging modes (all μ_2)[a]	η^1-*N*,η^1-*N*	η^2-*O*,(*N*),η^1-*N*	η^2-*N*,(*O*),η^1-*N*	η^2-*O*,(*N*),η^1-*N*	η^1-*N*,η^1-*N*	η^1-*N*,η^1-*N*	η^1-*N*,η^1-*N*	η^1-*N*,η^1-*N* η^1-*N*,η^1-*O*
T_{dec}, ° C	560	470	550	> 388	190[b]	250	570	285
color	purple	purple	green	green	dark purple	dark purple	white	cream-white
magnetism (J, cm^{-1})	−3.51 (canted-antiferromagnet)	−1.73	na[c]	−4.11	−36	−44		

[a] Parentheses highlight the long M···X contacts (see text). [b] The low decomposition temperature is related to the presence of perchlorate anions in its nanoporous framework. [c] Not available. [d] NH_4^+, ClO_4^-, H_2O in the cavities; nanoporous. [e] Hydrated; nanoporous.

similar in both the transition temperature ranges and enthalpy values. There are, however, significant differences in the thermal stability of the resulting microcrystalline M(pymo)$_2$ extended phases. While the Co(4-pymo)$_2$ crystalline phase is thermally stable well above its recrystallization (see Table 2), Ni(4-pymo)$_2$ possesses a significantly lower thermal stability, starting its decomposition process along with its recrystallization. Moreover, the latter system shows a decomposition temperature value *ca*. 200 °C lower than that of its 2-pymo analogue.[2b]

The lower thermal stability of the M(4-pymo)$_2$ systems compared to their M(2-pymo)$_2$ analogues is further substantiated by **1**, which shows a decomposition temperature value *ca*. 300 °C lower than that of its Zn(2-pymo)$_2$ analogue. In the latter case, the lower thermal stability of **1** can be partially related to its lower packing efficiency, illustrated by its higher V/Z value (Table 2). However, additional effects should be taken into account to explain the lower thermal stability for the 4-pymo systems: i.e. the asymmetric nature of the 4-pymo bridges which may facilitate the pyrimidine ring activation by the metal ions during the decomposition process.

The magnetic studies performed on **2** clearly show the presence of intermolecular antiferromagnetic coupling taking place between the Ni(4-pymo)$_2$(H$_2$O)$_4$ monomers, which agrees with its H-bonding supported polymeric nature. This result substantiates the efficiency of *X*-pymo bridges as transmitters of magnetic information even through noncovalent interactions. In the case of **3a**, the higher J exchange parameter value further supports the efficiency of 4-pymo bridges as transmitters of magnetic interactions. Moreover, it should also be noted the higher J value found in this case compared to the one found for the related Co(4-pymo)$_2$ material (see Table 2). This observation is an additional proof of N_3 involvement in Ni coordination and its concomitant octahedral coordination enviroment found in its electronic spectra and structure. Indeed, the *N*,*N*′-bridging mode is responsible for the much higher magnetic couplings, up to −44 cm^{-1} and −36 cm^{-1} for Cu(4-pymo)$_2$ and Cu(2-pymo)$_2$, respectively (Table 2).

Comparative Structural Analysis. From the analysis of the structural features of these systems, it can be easily seen that the presence of the exocyclic oxygen atom and particularly its location have a dramatic influence on the stereochemistry at the metal and on the overall packing types. For copper, the influence of the differently substituted ligands is "structurally" marginal but highly affects the shape, size, and hydrophilicity of the cavities.[9] For the remaining cations, O_1 becomes an "active" ligand and there is no structural analogy between the 2-pymo and 4-pymo derivatives (markedly different chromophores, pymo bridging modes, and supramolecular features being observed). For example, while cobalt, nickel, and zinc 2-pymo derivatives consist of slightly distorted diamondoid frameworks, (i) Co(4-pymo)$_2$ and Ni(4-pymo)$_2$, as discussed above, are based on 2D layers and (ii) Zn(4-pymo)$_2$, although 3D in nature, shows a *new*, rather distinct, framework topology.

According to the V/Z values reported in Table 2, we note that the two differently substituted pymo ligands have little effect on the structure compactness (apart from the Zn derivatives), even if binding in completely different modes and appearing in structures of markedly different dimensionality and density.

Finally, Figure 3 collects the relevant partial structures of M$_5$(X-pymo)$_4$ "clusters" highlighting the versatility of pymo ligands in terms of (i) hapticity (η^2 or η^3); (ii) bridging modes (*N*,*N*′ *vs N*,*O*), and (iii) relative orientation, resulting in a variety of coordination geometries of the metals and "clusters" shape.

Conclusions

The present contribution adds new information on the coordination chemistry of the 4-pymo ligand, which is still in its infancy. In particular, we reported the comparative analysis of the structural, thermal, and magnetic properties of a number of polymeric complexes with the 2- or 4-pymo ligands, highlighting important stereochemical differences. Work can be anticipated in the direction of preparing mixed ligand species, to assess the possible formation of solid solutions or segregation effects, and to move to different transition metal ions, in search for new polymeric architectures and functional materials (porous, sorptive, catalytic, and/or magnetic species).

In addition, the use of powder diffraction *from conventional laboratory equipment*, which made it possible to

structurally characterize a polycrystalline material, $Zn(2\text{-}pymo)_2$, with unexpected, and *new*, overall connectivity, is here emphasized.

Acknowledgment. The University of Insubria (Progetto di Ateneo 'Sistemi Poliazotati') and the Chamber of Commerce of Como (N.M. and S.G.), as well as the Spanish Ministerio de Ciencia y Tecnología (BQU2001-2955-CO2-1) and the Junta de Andalucía (E.B, J.A.R.N., and J.M.S.), are acknowledged for funding. E.B. also thanks the Spanish Ministerio de Educación, Cultura y Deporte, for a FPU grant. The courtesy of Dr. Davide Proserpio, who helped in the topological labeling of **1**, is also acknowledged.

Supporting Information Available: Crystallographic data in CIF format. This material is available free of charge via the Internet at http://pubs.acs.org.

IC0351287